Journal of Materials Chemistry B

ROYAL SOCIETY OF CHEMISTRY

PAPER

View Article Online
View Journal | View Issue

Cite this: J. Mater. Chem. B, 2026, 14, 2003

Facile synthesis of zeolitic imidazolate framework coated glass microspheres

Ashleigh M. Chester, †[a] Celia Castillo-Blas, ‡[a] John Luke Woodliffe,[b] Md Towhidul Islam,[b] Jesús Molinar-Díaz,[b] Andi Arjuna,[bc] Emma Barney,[b] Ifty Ahmed,[b] Andrea Laybourn, *[bd] David A. Keen[e] and Thomas D. Bennett *[af]

In this study we report a facile one-step, room temperature synthetic methodology for fabricating ZIF-8-coated phosphate-based glass (PBG) microspheres. ZIF-8 was grown *in situ* onto solid (non-porous) and porous P40 glass microspheres (composition $20Na_2O–24MgO–16CaO–40P_2O_5$, average diameter 153–172 μm), confirmed by PXRD and SEM analyses, with reaction times of one hour sufficient for coating onto solid P40 microspheres. An extended reaction time of 4.5 hours resulted in more homogeneous ZIF-8 coverage on the porous P40 microspheres. The ZIF-8 layer reduced microsphere degradation in water and slowed ion release from the microspheres, demonstrating a sacrificial protective coating effect of the ZIF-8. The ZIF-8 layer also enabled Zn^{2+} release (6.9–13.6 ppm over 7 days) and demonstrated improved methylene blue loading capacity, showing promise for pH-responsive drug delivery. This adaptable synthetic method to produce P40-based MOF composites highlights the potential synergistic benefits of combining PBG microspheres (bioactivity, tuneable degradation rates) and MOFs (high surface areas and porosity), offering an underexplored strategy to new MOF@PBG composites for drug delivery, antibacterial coatings and bone repair.

Received 30th October 2025,
Accepted 8th January 2026

DOI: 10.1039/d5tb02418h

rsc.li/materials-b

1. Introduction

Glass-based materials have diverse biomedical applications including anti-caries agents (agents for limiting tooth decay) in preventive dentistry,[1] sensors[2] and tissue engineering scaffolds, many of which comprise SiO_2 and P_2O_5 oxides.[3] Glasses are amorphous materials which transition from a brittle solid to a viscoelastic state over a distinct temperature range, given by the glass transition temperature (T_g).[4] Examples of potential bioactive glasses include phosphate-based glasses (PBGs), such as PBG microspheres (spherical particles with diameters from 1 to 1000 μm), which are fully resorbable and have tuneable degradation rates.[5–10] PBG microspheres offer size uniformity, favourable flow properties,[5] and improved control over degradation rate and release of incorporated molecules compared to other particle shapes.[5] For example, P40 glass microspheres, $20Na_2O–24MgO–16CaO–40P_2O_5$, have exhibited favourable cytocompatibility and biocompatibility responses and degradation rates, making them suitable for applications involving bone regeneration and targeted ion release, such as implant materials.[6,11]

P40 glass comprises equal proportions of Q^2 and Q^1 species (PO_4 groups interconnected *via* bridging oxygen atoms, $Q^1 = 1$ bridging oxygen, $Q^2 = 2$ bridging oxygens) and can be processed into microspheres *via* flame spheroidisation.[5] Incorporating a porogen (*e.g.* $CaCO_3$) prior to flame spheroidisation leads to pore formation, where pore size, porosity, and surface area can be modified by parameters such as porogen to glass ratio.[5] However, PBG microspheres can degrade rapidly in aqueous environments,[12] sometimes releasing glass fragments,[13] and their potential for drug delivery remains underexplored.[14]

Composites comprising microspheres or bioactive glasses are also evolving, such as those consisting of a metal–organic framework (MOF) as one component.[15–17] MOFs are hybrid materials containing metal ions and organic linkers which

[a] Department of Materials Science and Metallurgy, University of Cambridge, Cambridge, CB3 0FS, UK. E-mail: thomas.bennett@canterbury.ac.nz
[b] Advanced Materials Research Group, Faculty of Engineering, University of Nottingham, Nottingham NG7 2RD, UK
[c] Department of Pharmaceutical Sciences and Technology, Faculty of Pharmacy, Hasanuddin University, Makassar, 90245, Indonesia
[d] Institute of Process Research and Development & School of Chemistry, University of Leeds, Leeds, LS2 9JT, UK. E-mail: A.Laybourn@leeds.ac.uk
[e] ISIS Facility, Rutherford Appleton Laboratory, Harwell Campus, Didcot, Oxfordshire OX11 0QX, UK
[f] MacDiarmid Institute for Advanced Materials and Nanotechnology, School of Physical and Chemical Sciences, University of Canterbury, Private Bag 4800, Christchurch 8140, New Zealand
† Current address: UCL East, Marshgate, 7 Sidings Street, London, UK, E20 2AE.
‡ Current address: Institute of Materials Science of Madrid (ICMM-CSIC), Sor Juana Inés de la Cruz 3, 28049, Madrid, Spain.

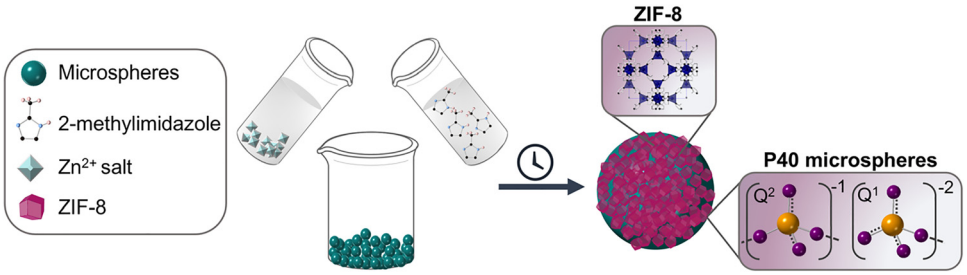

Fig. 1 Schematic showing the methodology used to synthesise ZIF-8@SMS and ZIF-8@PMS composites, SMS = solid microspheres and PMS = porous microspheres. ZIF-8 precursors were dissolved in methanol separately before they were added to a vial containing either solid microspheres or porous microspheres. Q^1 (1 bridging oxygen atom) and Q^2 (2 bridging oxygen atoms) units, which make up the P40 glass microspheres, are shown as tetrahedra with phosphorus and oxygen atoms represented by orange and purple spheres respectively. C, N, and H are represented by black, light blue and light pink in the 2-methylimidazole linker; Zn is represented by dark blue tetrahedra.

self-assemble into framework structures. Their tuneable chemistry, high surface areas, and controllable pore architectures make them attractive for biomedical applications such as drug delivery, biosensing, and bioimaging.[18] Previous studies combining MOFs with PBGs have demonstrated the advantages of the MOF component, such as increased surface areas,[19,20] improved air stability[20] and photocatalytic properties.[21] However, *in situ* growth of MOFs on PBGs, specifically on PBG microspheres, has not been extensively explored.

Recently, MOFs were grown onto iron calcium oxide microspheres to create magnetic framework composites with hierarchical porosity.[17] The methodology involved attaching polydopamine (PDA) and mercaptopyridine (MPYR) to the surface of porous magnetic microspheres (PMMs) to act as binders for *in situ* growth of two MOFs, HKUST-1, $[Cu_3(C_9H_6O_6)_2]$ and SIFSIX-3-Cu, $[Cu(C_4H_4N_2)_2(SiF_6)]$. The metal salt precursors and linker solutions were added to the functionalised PMMs for the self-assembly of MOFs onto the microspheres through a layer-by-layer method, which required multiple steps and functionalisation of the surfaces of the microspheres to create the MOF coating.

Here, we extend this concept to fabricate composites with solid and porous P40 microspheres and a prototypical MOF, ZIF-8, $[Zn(mIm)_2]$, where mIm = 2-methylimidazolate, which shows promise for drug delivery and wound healing applications,[22,23] using a facile, room temperature methodology (Fig. 1), combining the advantageous properties of P40 microspheres (bioactivity, tuneable degradation rates) and MOFs (high surface areas and porosity).[24] Optimisation of the synthesis, namely the reaction time, will be discussed and the stability tests required for the potential biomedical applications of these new composites will be explored.

2. Experimental methods

2.1. Materials

$Zn(OAc)_2{\cdot}2H_2O$ (≥98%) and 2-methylimidazole (99%) were purchased from Sigma Aldrich. Methanol (99.8%), calcium carbonate (98%) and phosphate buffer saline solution (PBS, pH 7.4, concentration 1×) were obtained from Fisher Scientific LTD. Methylene blue (MB) hydrate (≥97.0%) was purchased from Sigma Aldrich. Calcium hydrogen phosphate, magnesium hydrogen phosphate trihydrate, phosphorous pentoxide and sodium dihydrogen phosphate were obtained from Merck. All materials were used as received.

2.2. Microsphere synthesis

The P40 glasses were synthesised *via* melt-quenching, according to literature reports.[8] Sodium dihydrogen phosphate (NaH_2PO_4, 24 g), calcium hydrogen phosphate ($CaHPO_4$, 21.8 g), magnesium hydrogen phosphate trihydrate ($MgHPO_4{\cdot}3H_2O$, 41.8 g) and phosphorous pentoxide (P_2O_5, 56.8 g) were added to a platinum rhodium alloy crucible (Birmingham Metal Company, UK). The crucible was dried at 350 °C for 30 minutes. The mixture was then melted at 1150 °C for 1.5 hours and poured onto a steel plate and left to cool to room temperature. The P40 glass was ball milled (Retsch PM 100) and sieved into particle size ranges of 63–125 μm and 125–200 μm. The 125–200 μm particles were then processed using a flame spheroidisation process to prepare solid microspheres, using an oxy/acetylene flame spray gun (MK 74, Metallisation Ltd., UK). To synthesise porous microspheres, glass particles (63–125 μm) were mixed with calcium carbonate (porogen, ≤ 63 μm) in a 1 : 3 ratio and processed *via* flame spheroidisation. The porous phosphate glass microspheres were then washed using 5 M acetic acid for two minutes and then deionised water for five minutes to remove any unreacted $CaCO_3$ porogen from the microsphere products in line with our established washing protocol; insufficient washing can lead to remnant $CaCO_3$ (Calcite, CCDC 1865151) in the product.[7,25] The product was dried at 50 °C overnight. The resulting porous glass microspheres were sieved again to obtain microspheres with average particle sizes of 153 μm and 172 μm for the solid and porous microspheres, respectively.

2.3. Synthesis of ZIF-8@microsphere composites

The synthesis was carried out using a previously reported methodology.[26] $Zn(OAc)_2{\cdot}2H_2O$ (150 mg, 0.683 mmol) was added to methanol (2.5 mL). Separately, 2-methylimidazole (560 mg, 6.82 mmol) was added to methanol (2.5 mL) and sonicated to disperse the 2-methylimidazole particles. Solid microspheres (200 mg) were placed in a vial. The $Zn(OAc)_2{\cdot}$

$2H_2O$ solution and linker solution were poured over the microspheres for a reaction time of 1, 2 or 4.5 hours. White powder was collected by centrifugation at 4000 rpm for five minutes and washed twice with methanol (5 mL). The resulting product, ZIF-8@solid microsphere composites, denoted ZIF-8@SMS, was dried under vacuum overnight at 80 °C. The same procedure was used to synthesise ZIF-8@porous microsphere composites (denoted ZIF-8@PMS), using porous microspheres (200 mg) instead of solid microspheres.

2.4. Synthesis of ZIF-8 control

ZIF-8 synthesis in methanol and the associated changes in crystallite size and morphology have been characterised under various conditions.[26,27] Here, the ZIF-8 synthesis was based on a literature methodology with slight modifications.[28] Zinc acetate dihydrate (0.3 g, 1.367 mmol) was added to deionised water (5 mL). In a different vial, 2-methylimidazole (1.12 g, 14.495 mmol) was added to deionised water (5 mL) and sonicated. The zinc acetate dihydrate solution was then poured over the 2-methylimidazole solution and left at room temperature for 24 hours. White nanocrystals were collected by centrifugation at 4000 rpm for five minutes and were washed with methanol (3 × 20 mL). The product (~100 mg) was dried under vacuum overnight at 80 °C.

2.5. Powder X-ray diffraction measurements (PXRD)

PXRD data were collected using a B3 Bruker D8 DAVINCI diffractometer equipped with a position sensitive LynxEye detector. All samples were measured in Bragg–Brentano parafocusing geometry and Cu $K_{\alpha1}$ (λ = 1.5406 Å) radiation was used through a 0.012 mm Ni filter. Samples were compacted into 5 mm disks on a low background silicon substrate and measured in 1–50° 2θ range. Pawley refinements were completed using TOPAS academic (V7) software.[29] Thompson-Cox-Hastings pseudo-Voigt (TCHZ) peak shapes and a simple axial divergence correction were used for the refinements. The lattice parameters were refined using the crystallographic information file of ZIF-8 (CCDC number 947064),[30] in a 2θ range of 5–50°. The zero-point error was also refined.

2.6. Differential scanning calorimetry (DSC)

DSC measurements were performed using a NETSCH DSC 214 Polyma calorimeter. Approximately 5–10 mg of powdered samples were placed in sealed 70 μL aluminium crucibles with a pierced concave lid. Heating and cooling rates of 10 °C min^{-1} under argon were used, with background corrections applied. Heating cycles of 30–485 °C were used. Corrections were recorded prior to measurement using the same heating cycle on an empty aluminium crucible. An empty aluminium pan was used as a reference for all measurements and data were analysed using Netzsch Proteus® software package. Glass transition temperatures (T_gs) were determined using the Netzsch software.

2.7. Thermogravimetric analysis (TGA)

TGA thermograms were recorded using a TA instruments Discovery SDT 650 thermal analyser. Approximately 5–10 mg of powdered samples were placed in open 90 μL alumina crucibles and heated to 1000 °C at 10 °C min^{-1} under argon (flow rate: 100 mL min^{-1}), unless stated otherwise. All TGA data were analysed using TA Universal Analysis software.

2.8. Attenuated total reflectance-Fourier transform infrared spectroscopy (ATR-FTIR)

FTIR spectra were collected on a Nicolet iS50 FT-IR spectrometer in ATR mode between 400 and 4000 cm^{-1}. Several milligrams of powder were placed directly on the sample diamond plate. A background was subtracted from all spectra prior to each measurement.

2.9. Scanning electron microscopy-X-ray energy dispersive spectroscopy (SEM-EDS)

SEM images were collected using a high-resolution FEI Nova Nano SEM 450 electroscope. Samples were mounted on a flat aluminium stub with conductive carbon tape and coated with gold, unless stated otherwise in the figure captions. Working distances and accelerating voltages used for image collection were in the range of 5–15 kV and 5–10 mm respectively. An accelerating voltage of 15 kV was used for EDS analyses. For microsphere size analyses, XT Microscope Control software was used to measure the diameter of the microspheres (129–144 microspheres per sample) directly from the SEM images. Pore size diameters were determined from the SEM images using ImageJ software.[31] Four microspheres were analysed for the PMS (total no. of pores measured: 139).

2.10. Water degradation tests

Degradation analyses of the microspheres and composites were evaluated by mass loss measurements in ultra-pure water (water with a resistivity of 18.2 MΩ cm at 25 °C) in an oven at 37 °C for 30 days.[5] Approximately 50–52 mg of each sample was immersed in ultra-pure water (20 mL). The degraded microspheres and composites were removed from the media at various time points (1, 3, 7, 14, 21, and 30 days) *via* filtration before weighing. The ultra-pure water medium was refreshed after several days, where the microspheres were filtered before immersion in fresh medium.

2.11 pH and phosphate buffer saline (PBS) solution tests

Approximately 55 mg of each sample was immersed in PBS solution (20 mL). PBS 1× concentration was selected because it mimics the concentration of ions in the human body. The pH values (4–6 measurements) for each sample were determined at various time points (1, 2, 3, 6 and 8 days) using a Hanna instruments 2212 pH meter, calibrated using standard pH buffer solutions (pH 4.01 and 7.01).

2.12. Methylene blue (MB) dye uptake

MB was used here as a proxy for drug molecules. All samples were activated at 60 °C overnight prior to measurement. A 100 ppm stock solution of MB was prepared by dissolving MB hydrate (10 mg) in ultra-pure water (100 mL). The stock solution was diluted to give a 5 ppm solution. Each sample (10 mg) was added to 10 mL of 5 ppm solution and stirred for 24 hours at room temperature using a Grant-bio PTR-25 multi-function tube rotator. After 24 hours, the solids were removed *via* centrifugation and UV-VIS spectra of the filtrates were recorded. Calibrations were performed using variable MB solutions (0.25, 0.5, 1, 2, 3, 4, 5 mg L^{-1}), unless specified otherwise. Each sample was measured five times. A blank was recorded prior to measurement and all samples were measured at room temperature using rectangular polystyrene cuvettes with a total volume of 2.5 mL. All uptake studies were performed using the same starting concentration of 5 ppm, analyte concentration (1 mg/mL), and length of immersion in the dye solution (24 hours).

2.13. Ion release studies (ICP-MS) analyses

Mass loss and ion release of the samples were evaluated in ultra-pure water containing 1% w/v of sample (either pristine microspheres or composites) using ICP-MS. Each sample (100 mg) was immersed in ultra-pure water (10 mL) and incubated at 37 °C. Assessments were performed on days 1, 3 and 7. At each time point, 1 mL of the filtered solution (sampled using a 0.2 μm syringe filter) was diluted with 2% HNO_3 at a 1 : 10 ratio for ICP-MS analysis (Thermo-Fisher Scientific iCAP-Q equipped with collision cell technology with energy discrimination, UK). To maintain a constant volume, ultra-pure water (1 mL) was added to each vial before the vials were placed back in the incubator. Three replicates were analysed and the average values were reported. After 7 days, the solution was carefully removed from the vials using a syringe needle without removing any suspended solid. The remaining solution was then dried at 50 °C overnight and the samples were weighed using a precision balance (Sartorius CP 225D) to determine the percentage mass loss after 7 days incubation.

This method is modified from previously reported methodologies investigating ion release from P40 microspheres, namely a smaller sample mass was used and the samples were not agitated to avoid the potential loss of the attached MOF particles.[5]

3. Results and discussion

3.1. P40 characterisation and composite synthetic methodology

Both the solid and porous P40 microspheres were synthesised using reported procedures[8] and characterised by PXRD, FTIR spectroscopy, TGA and SEM-EDS analyses. PXRD analyses on the pristine porous (PMS) and solid microspheres (SMS) show diffuse scattering at $2\theta \sim 30^{\circ}$, consistent with the amorphous nature of the samples (Fig. S1a). The FTIR spectra of both the solid and porous microspheres shows broad bands, commonly observed for disordered glasses (Fig. S1b).[32] The band at 1112.6 cm^{-1} in the FTIR spectrum of the solid microspheres corresponds to asymmetric stretching of chain end Q^1 units (PO_3^{2-}).[33] Characteristic bands at 898.8 and 730 cm^{-1} correspond to symmetric and asymmetric stretching of P–O–P linkages respectively.[33] These bands are also present in the FTIR spectrum of PMS at similar positions.

SEM analyses of both the solid and porous microspheres show a distribution of spherical particle sizes sampled over various regions (129–142 spheres per sample) (Fig. S2–S4) with mean particles sizes of 153 ± 25 μm and 172 ± 21 μm for SMS and PMS, respectively; microsphere diameter distributions are expected from the synthesis and have been reported previously.[12] Additionally, PMS exhibits a distribution of pore diameters (ranging from 1.2–43.4 μm), with average pore diameters of 8.7 ± 7.1 μm (Fig. S5 and S6). The pore diameters determined are consistent with previous studies on P40-Fe_3O_4 microspheres where a range of 0.9–56.2 μm was reported.[8] SEM-EDS was used to determine the compositions of the glasses (Table S1 and Fig. S7 and S8), giving negligible deviations from the nominal composition of Mg, Na, and P in both the solid and porous microspheres.

TGA thermograms of pristine SMS show negligible mass losses up to 1000 °C (Fig. S9). Negligible mass loss in the temperature range of the TGA measurement is observed for PMS (Fig. S10). DSC analyses on the pristine porous and solid microspheres indicate very similar T_gs at 450 °C (SMS) and 447 °C (PMS), in line with reported values (Fig. S11 and S12).[11] A small difference in T_g between the solid and porous microspheres is expected, given the minor change in formulation from incorporation of CaO from porogen break down.[5]

Composites consisting of ZIF-8 coated microspheres were synthesised according to the schematic in Fig. 1. ZIF-8 precursors, $Zn(OAc)_2.2H_2O$ and 2-methylimidazole ($C_4H_6N_2$), were dissolved in methanol and added to the porous and solid microspheres in separate experiments (see Experimental Methods). Syntheses were carried out in methanol to avoid dissolution of the microspheres in aqueous media. The resulting composites were termed ZIF-8@SMS_*x*hr (SMS = solid microspheres) and ZIF-8@PMS (PMS = porous microspheres), where *x*hr refers to the duration of the synthesis. Successful growth of ZIF-8 on the microspheres was primarily monitored by SEM, because the low concentration of MOF on the spheres hinders its detection by alternative techniques.[17] Post synthesis, the composites were washed twice with methanol (~5 mL) and the solid powder was isolated *via* centrifugation.

3.2. Evaluating reaction time for ZIF-8@solid microspheres composites

The reaction time was optimised to obtain a homogeneous layer of ZIF-8 on the surfaces of the microspheres. Selection of the reaction time encompasses a compromise between allowing enough time for ZIF-8 growth on the surfaces of the microspheres and preventing potential degradation or dissolution of

the microspheres in methanol. Initially, composites with solid microspheres were synthesised with a reaction time of 4.5 hours. SEM images of the ZIF-8@SMS_4.5hr composite show the formation of rhombic dodecahedron shaped[26] ZIF-8 particles <1 μm on the surface of the microspheres (Fig. S13). Crucially, these images were taken post washing which indicates that the ZIF-8 was robustly attached to the microspheres' surfaces; possible interactions include those between zinc from ZIF-8 and the phosphate groups in the glass, which have been observed previously in ZIF-8/PBG composites.[19]

However, ZIF-8 agglomeration on the surfaces of the microspheres suggests an overly long reaction time, resulting in aggregation instead of uniform coating. The reaction time was therefore reduced to two hours to minimise this prolific growth, however SEM images of the SEM ZIF-8@SMS_2hr composite display the same agglomeration (Fig. S14). The reaction time was further reduced to alleviate these issues. SEM images for the composite produced after one hour of synthesis (Fig. 2) show successful coating of ZIF-8 on the surface of the spheres, without agglomeration observed in the 2 and 4.5 hour samples (Fig. S13 and S14).

3.3. Evaluating reaction time for ZIF-8@porous microspheres composites

The same reaction durations (1, 2 and 4.5 hours) were used to synthesise the ZIF-8@porous microspheres composites. SEM images of the resulting composites were analysed to determine the optimum reaction time. Although 1 hour was sufficient for ZIF-8 to grow on the surface and inside the pores of several spheres for the ZIF-8@PMS_1hr composite, others show minimal ZIF-8 coating (Fig. S15 and S16), which can be ascribed to the increased surface area of the PMS sample relative to its solid counterparts. Doubling the reaction time resulted in a more homogenous ZIF-8 coating on the surfaces of the microspheres (Fig. S17). However, SEM images of the ZIF-8@PMS_2hr composite show gaps in the ZIF-8 coating on the surfaces of some of the spheres. SEM images of the ZIF-8@PMS_4.5hr composite show improved coating of ZIF-8 on several of the spheres, with minimal aggregation of ZIF-8 (Fig. 3).

Based on the SEM results, the ZIF-8@SMS_1hr and ZIF-8@PMS_4.5hr composites were characterised further and evaluated under biologically relevant conditions (pH 7.4, 37 °C).

3.4. Composite characterisation

The ZIF-8@SMS_1hr and ZIF-8@PMS_4.5hr composites were analysed by PXRD (including Pawley refinement), FTIR spectroscopy, DSC and TGA. Pawley refinements of the PXRD patterns of the ZIF-8@SMS_1hr and ZIF-8@PMS_4.5hr composites (Table S2 and S3 and Fig. S18 and S19) show an amorphous background from the microspheres and ZIF-8 peaks observed in the ZIF-8 control (Table S4 and Fig. S21). FTIR spectra of the composites show bands corresponding to P40 glass with the presence of additional, sharper bands from ZIF-8 (Fig. S20); for example the characteristic C=N stretch of ZIF-8 is present at ~1583.1 cm^{-1} for both composites. Bands in the ZIF-8@SMS_1hr spectrum at 1422.7 cm^{-1} and 1310.4 cm^{-1} are related to ring stretching of the 2-methylimidazolate linker; the same bands are present at 1423 cm^{-1} and 1309.6 cm^{-1} in the ZIF-8@PMS_4.5hr composite spectrum. Additional bands in the ZIF-8@SMS_1hr composite spectrum are present at 1146.5 cm^{-1}, 994.2 cm^{-1}, and 758.9 cm^{-1}, ascribed to C–N stretching of the organic linkers. These bands are also present in the ZIF-8@PMS_4.5hr composite spectrum at similar wavenumbers (1146 cm^{-1}, 993.4 cm^{-1}, and 758.7 cm^{-1}).[34,35] Furthermore, sharper bands are also present in the 600–800 cm^{-1} region in both composites, associated with C–H stretching in ZIF-8. The presence of these sharper bands agrees with the PXRD and SEM results, which both indicate successful growth of ZIF-8 on the surfaces of porous and solid microspheres.

The thermal properties of the composites were assessed by TGA (Fig. S22–S25) and DSC (Fig. S26–S28). TGA of the

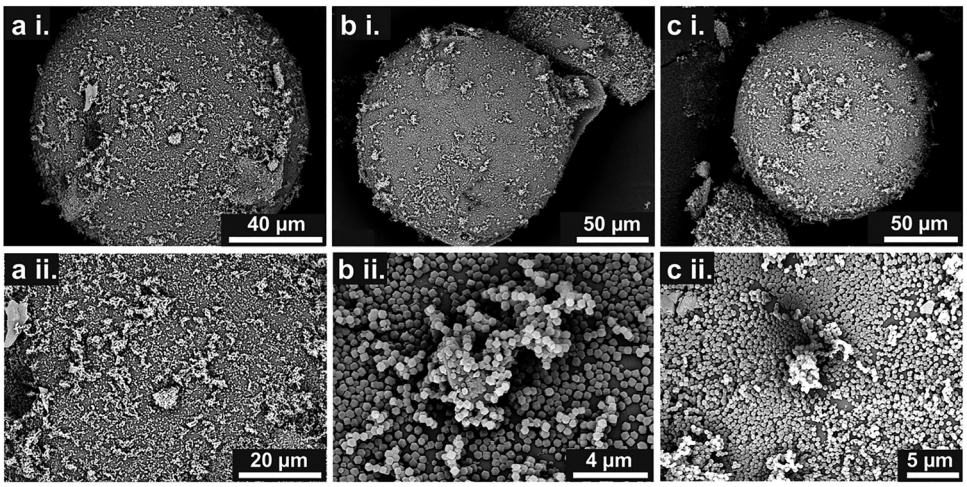

Fig. 2 SEM images of the ZIF-8@SMS_1hr composite. Three different spheres are shown in images (a) i, (b) i and (c) i. Images (a) ii, (b) ii and (c) ii correspond to the same spheres in (a) and (b) and (c) but at higher magnification.

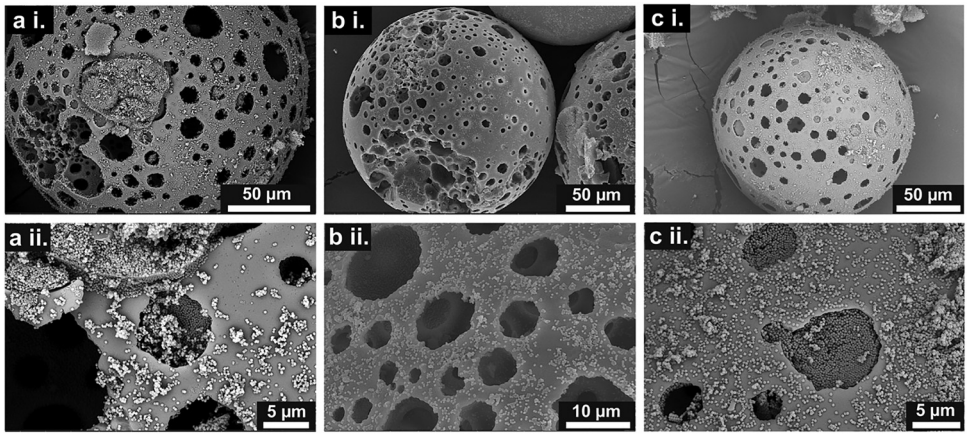

Fig. 3 SEM images of the ZIF-8@PMS_4.5hr composite showing three different spheres, (a) i (BSE imaging mode), (b) i (SE imaging mode) and (c) i (BSE imaging mode). Images (a) ii, (b) ii and (c) ii correspond to the same spheres but at higher magnification. SE and BSE refer to secondary electron and backscattered electron imaging modes.

ZIF-8@SMS_1hr and ZIF-8@PMS_4.5hr composites show T_ds of 548 °C and 522 °C, close to the T_d (~514 °C) of pristine ZIF-8, indicative of negligible difference in thermal stability of ZIF-8 in the composites relative to pristine ZIF-8. From TGA analysis of the ZIF-8 control, the amount of ZIF-8 coated onto the microspheres' surfaces was estimated to be 4.51 wt% and 4.54 wt% on the ZIF-8@SMS_1hr and ZIF-8@PMS_4.5hr composites, respectively. The second DSC upscans of the ZIF-8@SMS_1hr and ZIF-8@PMS_4.5hr composites display T_gs at 452 °C and 447 °C, respectively, indicating preservation of P40 glass in the composites after synthesis.

3.5. Assessing suitability for biomedical applications

The potential suitability of ZIF-8@microsphere composites for biomedical applications was assessed using water degradation analysis, pH testing in phosphate-buffered saline (PBS) solution (pH 7.4), dye uptake, and ion release studies. The effect of the ZIF-8 coating was explored by comparing the ZIF-8@SMS_1hr composite to the pristine SMS in the water degradation analyses and PBS studies.

3.5.1. Water degradation analyses. Dissolution profiles of PBGs result in ion release (phosphate ions, Ca^{2+}, Mg^{2+} and Na^{+} *etc.*..) which can be tailored for specific applications such as degradable bone repair implants. Degradation rates are therefore crucial for controlled release of therapeutic agents[36,37] and evaluating material suitability for scenarios such as bone repair supports where the support must remain intact until new tissue has formed.[6] Degradation rates of PBG microspheres can also affect tissue response and excess release of ions can cause cell death (cytotoxicity).[13] A potential benefit of a ZIF-8 coating is protecting the microspheres from fast degradation, which is often associated with surface damage on glass implants, and the release of glass fragments/particulates from degradation can adversely affect cells in culture.[13]

Water degradation tests of SMS and ZIF-8@SMS_1hr composite were carried out by immersion in ultra-pure water over 30 days at 37 °C (Experimental Methods). PXRD patterns of both samples show the presence of calcite, $CaCO_3$ (CCDC number 1865151)[25] post-immersion (Fig. S29b), which can grow on the surfaces of bioactive glasses when calcium ions released from the glass degradation react with HCO_3^- from the dissolution of atmospheric CO_2.[38] These peaks are present in lower relative intensity for the ZIF-8@SMS_1hr composite compared with pristine water-exposed SMS. There is an absence of ZIF-8 Bragg peaks in the PXRD pattern of the ZIF-8@SMS_1hr composite, suggesting ZIF-8 degradation, which occurs in water at ambient conditions.[39]

SEM images of the ZIF-8@SMS_1hr composite show that the spheres remain intact, but surface cracks are evident after 30 days immersion (Fig. S30). Additionally, the morphology of the ZIF-8 particles changed after immersion, with the originally rhombic-dodecahedron shaped particles becoming rounded, suggesting partial dissolution of the crystallites in the aqueous medium. Degradation of ZIF-8 in water can be accompanied by morphology changes of the crystallites.[39] The ZIF-8 coating in this study modifies the surfaces of the microspheres, where rougher surfaces can potentially enhance cell adhesion[40] and increase the specific surface area of the material, which would be beneficial for cell adhesion, nutrient transport, and protein binding.[13,40]

Mass loss in water for the ZIF-8@SMS_1hr composite was lower than that of the pristine solid microspheres after 30 days (48% and 70% respectively, Fig. S29a and Table S5), likely resulting from the ZIF-8 coating degrading initially, before degradation of the solid microspheres. This is evidenced by SEM images of the ZIF-8@SMS_1hr composite after water degradation tests, which show morphological changes in the ZIF-8 particles and appearance of cracks on the surfaces of the microspheres (Fig. S30). Benefits of slower degradation of the ZIF-8@SMS_1hr composite relative to SMS could include tailored ion and drug release, depending on the targeted application. Previous studies have demonstrated that the faster degradation rates of P40 microspheres, relative to other PBG microsphere formulations, are linked with potentially adverse effects on tissue response,[6] and SEM studies have shown crack

formation and delamination on the surfaces of glass microspheres, which can affect cell attachment and proliferation.[6,13]

3.5.2. PBS studies. PBS solution is widely used for biomedical and cell cultivation studies, primarily because its pH is kept constant at 7.4 (physiological pH),[37] and it has been used to study the biodegradability of several MOFs such as UiO-67, ZIF-7 and HKUST-1.[41] Importantly, the drug release performance of ZIF-8 is linked to its degradation under physiological conditions, where changes in morphology and/or structural degradation can lead to different rates of drug release.[36,37] Previous studies have confirmed the degradation of ZIF-8 in PBS at 37 °C, where changes in particle morphology were observed.[36,37] This is associated with linker release and changes in Zn^{2+} coordination environment, which can be catalysed by phosphate ions, such as $[HPO_4]^{2-}$, contained in PBS.[42]

The pH of a pristine ZIF-8 control, the solid microspheres, and the ZIF-8@SMS_1hr composite was monitored at several time points over an 8-day period. The solution of solid microspheres shows minimal deviation from pH 7.4 over 8 days (Fig. S31a), whereas the ZIF-8@SMS_1hr composite shows an increase in pH from 7.4 to 8.7 over 8 days. For comparison, pristine ZIF-8 immersed in PBS results in an increase in pH from 8.4 to 9.5 over 8 days. SEM images of the ZIF-8@SMS_1hr composite after eight days immersion in PBS shows morphological changes to the ZIF-8 coating, consistent with previous studies on ZIF-8[36,37] and is indicative of MOF dissolution. As with immersion in ultra-pure water for 30 days, the microspheres retain their spherical morphology and cracks are evident when immersed in PBS for 8 days (Fig. S32); however, their surfaces have been modified by ZIF-8 degradation.

PXRD analyses of the samples after immersion in PBS show no changes to the pristine solid microsphere sample (Fig. S31b), however, the ZIF-8 peaks in the ZIF-8@SMS_1hr composite have disappeared almost entirely, except for a peak at $2\theta \sim 7.5°$. This result is consistent with degradation studies of ZIF-8 in PBS at 37 °C which showed that the ZIF-8 (110) Bragg peak at $2\theta = 7.34°$ decreased with incubation time in PBS over a 24-hour period.[37] This (110) Bragg peak is also absent after 30 days immersion in ultra-pure water (Fig. S31b). However, ZIF-8 rhombohedra particles are still visible on the surfaces of the microspheres, indicating ZIF-8 presence post immersion, but with a partially collapsed microstructure.

Overall, the changes in pH are consistent with SEM and PXRD results showing degradation of ZIF-8 under biologically relevant conditions and is in line with previous reports,[36,37] which could be useful for release of an encapsulated drug from the pores of ZIF-8.[43]

3.5.3. Dye uptake. The direct use of therapeutic drugs often suffers from poor drug stability, non-specific targeting,[24] and undesired side effects arising from increased dosages. To address this, studies have investigated the suitability of ZIF-8 as a drug delivery agent[24] for *e.g.* doxorubicin,[44] curcumin,[45] 5-fluorouracil, and ibuprofen.[22] Additionally, composites containing ZIF-8 have been designed for drug loading and controlled release.[46,47] Here, the dye methylene blue (MB) was used as a proxy for drug molecules to assess the drug delivery potential of the ZIF-8@SMS_1hr and ZIF-8@PMS_4.5 hr. MB was selected because of its sharp peak in the visible region (~660–668 nm) and reliable signal (Fig. 4).

The solid microspheres and ZIF-8@SMS_1hr composite display MB uptakes of 11.3% (0.56 ppm) and 16.5% (0.82 ppm), respectively; the composite displays a 46% increase relative to the SMS starting material (Table S6). The pristine porous microspheres show an MB uptake of 18.7% (0.93 ppm) while the ZIF-8@PMS_4.5hr composite exhibits an uptake up 24.6% (1.23 ppm), an increase of 32% relative to the pristine porous microspheres (Table S7).

Although the absolute values suggest only minor improvements, the mass of ZIF-8 on the microspheres is low; approximately 4.51 wt% for the ZIF-8@SMS_1hr composite and 4.54 wt% for the ZIF-8@PMS_4.5hr composite, based on the TGA results (Fig. S22–S25). Nonetheless, these data show that coating the microspheres with ZIF-8 leads to an appreciable increase in uptake, despite the small amount of ZIF-8 on their

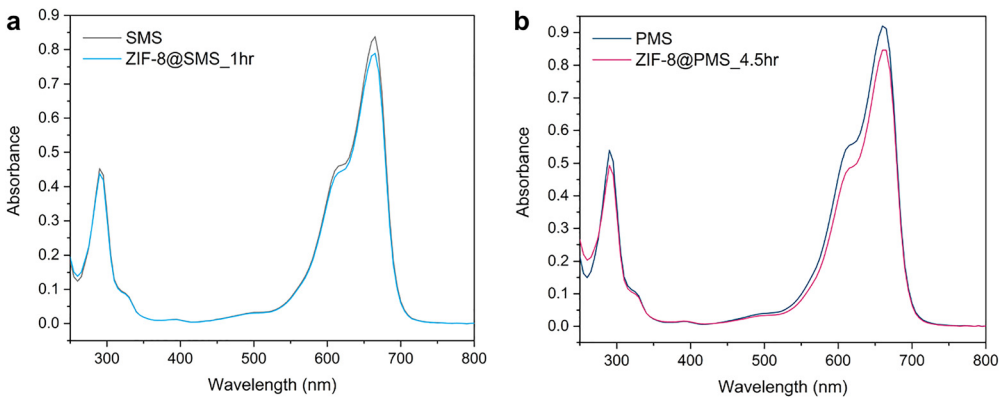

Fig. 4 Methylene blue (MB) absorbance at 665 nm for MB solutions in contact (over a 24-hour period) with (a) SMS and the ZIF-8@SMS_1hr composite and (b) PMS and the ZIF-8@PMS_4.5hr composite. Absorbances and calculated uptake can be found in the Supplementary information, Tables S6 and S7, Fig. S33 and S34.

surfaces. Additionally, increasing the reaction time for the PMS composites could improve the uptake by producing a more homogenous ZIF-8 coating with greater coverage on the microsphere surfaces and within their pores.

3.5.4. Ion release studies in water. Ion release studies in ultra-pure water were performed on the composites and microspheres for phosphate anions and biologically active Na^+, Mg^{2+} and Ca^{2+}, exploiting the fact that PBGs are fully resorbable in aqueous environments. Additionally, the release of Zn^{2+} ions, which have demonstrable anti-inflammatory and antibacterial activity, was assessed because potential bioactivity of ZIF-8 has been linked to its porous structure and source of Zn^{2+}.[48] The composites and pristine microspheres were immersed in ultra-pure water at 37 °C and the ion release profiles were measured using ICP-MS (Fig. 5).

The ion release of [Na] (32.1 ± 1.1 ppm), [Mg] (22 ± 0.6 ppm) and [P] (80.8 ± 2.4 ppm) from the pristine SMS sample is similar to that reported after 7 days; the release of [Ca] deviates from reported values (16.9 ± 1.1 ppm).[49] Discrepancies such as lower ion concentrations on days 3 and 7 compared to some studies for SMS and PMS samples ([Na] ~60–70 ppm, [P] ~125–190 ppm, [Mg] ~28–38 ppm after 7 days)[12] were observed for both SMS and PMS samples, likely because of the different media, starting concentrations and conditions, and dilution effect (see Experimental Methods).[5]

For all ions except Ca^{2+}, which is released in a similar amount after 7 days (16.9 ± 1.1 ppm and 15.9 ± 1.1 ppm for SMS and PMS, respectively), the pristine porous microspheres released more ions than their solid counterparts, which was expected because of the increased surface area exposed to the water media, a trend observed previously.[5] The release of Ca^{2+} from the SMS sample is slightly higher than the PMS sample, which has also been observed previously.[5]

The ZIF-8@SMS_1hr composite releases lower concentrations of Na^+, Mg^{2+}, phosphate ions and Ca^{2+} ([Na] 25.7 ± 1.9 ppm, [Ca] 7.7 ± 0.5 ppm, [Mg] 16.3 ± 1.5 ppm, [P] 51.7 ± 4.2 ppm on day 7) compared to pristine SMS (Fig. 5a–d and Fig. S35). These values indicate a protective coating effect of the ZIF-8 particles on the surfaces of the microspheres, which is attractive for applications requiring slow ion/drug release and controlled degradation of the microspheres. This effect is not evident for PMS or the ZIF-8@PMS_4.5hr composite, where comparable concentrations of Na^+, Mg^{2+} and phosphate ions are observed for both samples (Fig. 5a–c) on days 1, 3, and 7 ([Na] 59.8 ± 6.5 ppm, [Ca] 12.2 ± 0.8 ppm, [Mg] 33.9 ± 2.9 ppm, [P] 117.9 ± 10.3 ppm on day 7 for the ZIF-8@PMS_4.5hr composite). This effect likely results from insufficient time for the ZIF-8 particles to coat the PMS sample, which has a higher surface area relative to its solid counterpart, and given a similar wt% of ZIF-8 is coated on the solid and porous microspheres, less of the PMS surface is protected due to its higher surface area. Moreover, the restricted pore connectivity of the PMS could affect the ability of the MOF to grow efficiently within the pores.

The release of Zn^{2+} is higher for the ZIF-8@SMS_1hr composite (13.6 ± 0.3 ppm) compared to the ZIF-8@PMS_4.5hr composite (6.9 ± 1.1 ppm) on day 7 (Fig. 5e), again likely caused by the more homogenous coating of ZIF-8 on the ZIF-8@SMS_1hr composite relative to the ZIF-8@PMS_4.5hr composite. The release of Zn^{2+} ions are promising for introducing antimicrobial activity to the microspheres, where the concentrations on day

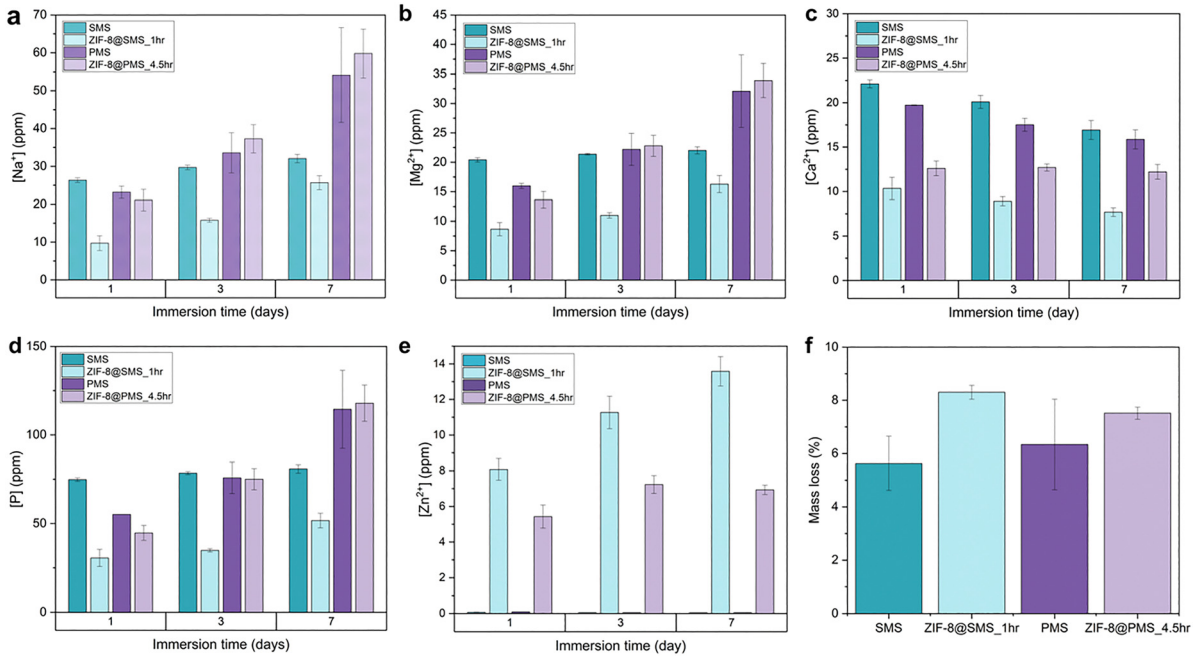

Fig. 5 Ion release profiles and mass loss of the pristine microspheres and composites over a 7-day period, (a) $[Na^+]$, (b) $[Mg^{2+}]$, (c) $[Ca^{2+}]$, (d) [P], (e) $[Zn^{2+}]$ and (f) mass loss after 7 days. [P] refers to all ionic forms of phosphorus (*e.g.* $[PO_4^{3-}]$, $[HPO_4^{2-}]$, $[H_2PO_4^-]$) detected by ICP-MS.

7 fall within the recommended Zn^{2+} ion concentration of between 0.65 and 16.25 ppm.[40]

The mass loss (%) calculated for the SMS (6.7%) and ZIF-8@SMS_1hr composite (8%) differs from the water degradation studies (31% for SMS and 21.8% for the ZIF-8@SMS_1hr composite on day 7); a plausible explanation is the different sample concentrations used for the studies, because ZIF-8 degradation depends on ZIF-8 mass:water ratio.[39,50]

4. Conclusions

In this work, we describe the rapid one-pot growth of ZIF-8 on solid and porous P40 glass microspheres. Water degradation studies showed reduced mass loss of the ZIF-8@SMS_1hr composite (48%) relative to SMS (70%) after 30 days, indicating potential protective effects of the ZIF-8 coating. Immersion of the ZIF-8@SMS_1hr composite and SMS in PBS (1×) solution led to an increased pH of the PBS solution (from 7.4 to 8.6 over 8 days) and PXRD and SEM images showed ZIF-8 degradation from the surfaces of the microspheres. These findings align with the water degradation results and suggest the potential of the ZIF-8@SMS composite to deliver drug molecules *via* ZIF-8 degradation.

To evaluate drug-delivery potential, methylene blue uptake was measured for the pristine microspheres and the ZIF-8 composites. The ZIF-8@SMS_1hr composite showed a 46% increase in uptake (16.5% *vs.* 11.3% for SMS), while ZIF-8@PMS_4.5hr exhibited a 32% increase (24.6% *vs.* 18.7% for PMS). These results indicate that even low ZIF-8 loadings (~4.5 wt%) significantly enhance dye uptake. Ion release studies showed that the ZIF-8@SMS_1hr composite released less ions (Mg^{2+}, Na^{+}, Ca^{2+} and phosphate ions) than the pristine solid microspheres after one week, indicating a protective effect of the ZIF-8 coating on the surfaces of the microspheres. Additionally, both the ZIF-8@SMS_1hr composite and ZIF-8@PMS_4.5hr composites exhibited release of Zn^{2+} after 7 days immersion.

Future work will focus on optimising ZIF-8 loading and evaluating drug encapsulation and release under physiologically relevant conditions. Through such efforts, ZIF-8–functionalised glass microspheres may advance as versatile platforms for therapeutic delivery and can be extended to other phosphate-based glass materials with different morphologies depending on the desired application, where the ease and adaptability of the method can be exploited.

Author contributions

CCB, AMC, LW, AL, IA, and TDB conceptualised the project. AMC wrote the manuscript with contributions from all authors. ZIF-8 and composite samples were synthesised by AMC and CCB. The P40 glass microspheres were synthesised by LW, MTI, JM, and AA. AMC and CCB analysed the P40 glass microspheres. PXRD and DSC were performed by AMC and CCB. FTIR, TGA, Pawley refinements, and SEM analyses were performed by AMC. Water degradation analyses were performed by AMC and CCB. AMC completed the pH/PBS studies and methylene blue uptake studies. MTI conducted the ICP-MS (ion release) studies, in conjunction with Saul Vazquez Rein. EB provided useful feedback. DAK, TDB, IA, and AL supervised the project and acquired funding.

Conflicts of interest

There are no conflicts to declare.

Data availability

Experimental data in support of the findings of this study are provided in the paper, in the Supplementary information (SI), or are openly available from the University of Cambridge repository at https://doi.org/10.17863/CAM.119282. Supplementary information is available. See DOI: https://doi.org/10.1039/d5tb02418h.

Acknowledgements

AMC and CCB acknowledge Leverhulme Trust Research Project Grant (RPG-2020-005). TDB thanks the Royal Society for both a University Research Fellowship (URF\R\211013) and a research grant (RGS\R2\212221). AMC and MTI acknowledge Saul Vazquez Rein at the School of Biosciences, University of Nottingham, for ICP-MS analysis. JM-D thanks the Engineering and Physical Sciences Research Council (EPSRC), as part of the "EPSRC Future Composites Manufacturing Research Hub" [EP/P006701/1]. LW acknowledges funding from the Engineering and Physical Sciences Research Council (EPSRC) for his Doctoral Prize Fellowship (Grant Number: EP/W524402/1). The authors also acknowledge funding from the Faculty of Engineering at the University of Nottingham and from the Engineering and Physical Sciences Research Council (EPSRC) and Science Foundation Ireland (SFI) Centre for Doctoral Training in Sustainable Chemistry: Atoms-2-Products an Integrated Approach to Sustainable Chemistry (Grant Number: EP/S022236/1). AL gratefully acknowledges financial support from a UKRI Future Leaders Fellowship (MR/Y018087/1).

References

1 E. A. Mahdy, Z. Y. Khattari, W. M. Salem and S. Ibrahim, *Mater. Chem. Phys.*, 2022, **286**, 126231.
2 S. Oguzlar, M. Zeyrek Ongun and A. M. Deliormanlı, *ACS Omega*, 2023, **8**, 40561–40571.
3 L.-C. Gerhardt and A. R. Boccaccini, *Materials*, 2010, **3**, 3867–3910.
4 E. Refstrup and J. Bonke, *Encyclopedia of Dairy Sciences*, Elsevier, 2011, pp. 208–215.
5 K. M. Z. Hossain, U. Patel, A. R. Kennedy, L. Macri-Pellizzeri, V. Sottile, D. M. Grant, B. E. Scammell and I. Ahmed, *Acta Biomater.*, 2018, **72**, 396–406.

6 J. S. MLaren, L. Macri-Pellizzeri, K. M. Z. Hossain, U. Patel, D. M. Grant, B. E. Scammell, I. Ahmed and V. Sottile, *ACS Appl. Mater. Interfaces*, 2019, **11**, 15436–15446.
7 S. A. Samad, A. Arafat, R. Ferrari, R. L. Gomes, E. Lester and I. Ahmed, *Int. J. Appl. Glass Sci.*, 2022, **13**, 63–81.
8 J. Molinar-Díaz, J. L. Woodliffe, B. Milborne, L. Murrell, M. T. Islam, E. Steer, N. Weston, N. A. Morley, P. D. Brown and I. Ahmed, *Adv. Mater. Interfaces*, 2023, **10**, 2202089.
9 N. J. Lakhkar, J.-H. Park, N. J. Mordan, V. Salih, I. B. Wall, H.-W. Kim, S. P. King, J. V. Hanna, R. A. Martin, O. Addison, J. F. W. Mosselmans and J. C. Knowles, *Acta Biomater.*, 2012, **8**, 4181–4190.
10 T. Tang, P. Kang, F. Verisqa, L. Nguyen and J. C. Knowles, *J. Biomed. Mater. Res.*, 2024, **112**, 2314–2328.
11 U. Patel, L. Macri-Pellizzeri, K. M. Zakir Hossain, B. E. Scammell, D. M. Grant, C. A. Scotchford, A. C. Hannon, A. R. Kennedy, E. R. Barney, I. Ahmed and V. Sottile, *J. Tissue Eng. Regener. Med.*, 2019, **13**, 396–405.
12 M. T. Islam, L. Macri-Pellizzeri, K. M. Z. Hossain, V. Sottile and I. Ahmed, *Mater. Sci. Eng., C*, 2021, **120**, 111668.
13 D. Gupta, K. M. Z. Hossain, M. Roe, E. F. Smith, I. Ahmed, V. Sottile and D. M. Grant, *ACS Appl. Bio Mater.*, 2021, **4**, 5987–6004.
14 J. Molinar-Díaz, A. Arjuna, N. Abrehart, A. McLellan, R. Harris, M. T. Islam, A. Alzaidi, C. R. Bradley, C. Gidman, M. J. W. Prior, J. Titman, N. P. Blockley, P. Harvey, L. Marciani and I. Ahmed, *Molecules*, 2024, **29**, 4296.
15 A. R. Boccaccini, M. Erol, W. J. Stark, D. Mohn, Z. Hong and J. F. Mano, *Compos. Sci. Technol.*, 2010, **70**, 1764–1776.
16 M. Araújo, R. Viveiros, A. Philippart, M. Miola, S. Doumett, G. Baldi, J. Perez, A. R. Boccaccini, A. Aguiar-Ricardo and E. Verné, *Mater. Sci. Eng., C*, 2017, **77**, 342–351.
17 J. L. Woodliffe, J. Molinar-Díaz, M. T. Islam, L. A. Stevens, M. D. Wadge, G. A. Rance, R. Ferrari, I. Ahmed and A. Laybourn, *J. Mater. Chem. A*, 2023, **11**, 14705–14719.
18 M. Hefayathullah, S. Singh, V. Ganesan and G. Maduraiveeran, *Adv. Colloid Interface Sci.*, 2024, **331**, 103210.
19 C. Castillo-Blas, A. M. Chester, R. P. Cosquer, A. F. Sapnik, L. Corti, R. Sajzew, B. Poletto-Rodrigues, G. P. Robertson, D. J. M. Irving, L. N. McHugh, L. Wondraczek, F. Blanc, D. A. Keen and T. D. Bennett, *J. Am. Chem. Soc.*, 2023, **145**, 22913–22924.
20 A. M. Chester, C. Castillo-Blas, R. Sajzew, B. P. Rodrigues, G. I. Lampronti, A. F. Sapnik, G. P. Robertson, M. Mazaj, D. J. M. Irving, L. Wondraczek, D. A. Keen and T. D. Bennett, *Dalton Trans.*, 2024, **53**, 10655–10665.
21 C. Castillo-Blas, M. J. García, A. M. Chester, M. Mazaj, S. Guan, G. P. Robertson, A. Kono, J. M. A. Steele, L. León-Alcaide, B. Poletto-Rodrigues, P. A. Chater, S. Cabrera, A. Krajnc, L. Wondraczek, D. A. Keen, J. Alemán and T. D. Bennett, *ACS Appl. Mater. Interfaces*, 2025, **17**, 15793–15803.
22 P. H. Ho, F. Salles, F. Di Renzo and P. Trens, *Inorg. Chim. Acta*, 2020, **500**, 119229.
23 S. Yao, J. Chi, Y. Wang, Y. Zhao, Y. Luo and Y. Wang, *Adv. Healthcare Mater.*, 2021, **10**, 2100056.
24 Q. Wang, Y. Sun, S. Li, P. Zhang and Q. Yao, *RSC Adv.*, 2020, **10**, 37600–37620.
25 N. Ishizawa, H. Setoguchi and K. Yanagisawa, *Sci. Rep.*, 2013, **3**, 2832.
26 C. Avci, J. Ariñez-Soriano, A. Carné-Sánchez, V. Guillerm, C. Carbonell, I. Imaz and D. Maspoch, *Angew. Chem., Int. Ed.*, 2015, **54**, 14417–14421.
27 T. V. Tran, H. H. Dang, H. Nguyen, N. T. T. Nguyen, D. H. Nguyen and T. T. T. Nguyen, *Nanoscale Adv.*, 2025, **7**, 3941–3960.
28 L. Sheng, F. Yang, C. Wang, J. Yu, L. Zhang and Y. Pan, *Mater. Lett.*, 2017, **197**, 184–187.
29 A. A. Coelho, *J. Appl. Crystallogr.*, 2018, **51**, 210–218.
30 O. Karagiaridi, M. B. Lalonde, W. Bury, A. A. Sarjeant, O. K. Farha and J. T. Hupp, *J. Am. Chem. Soc.*, 2012, **134**, 18790–18796.
31 C. A. Schneider, W. S. Rasband and K. W. Eliceiri, *Nat. Methods*, 2012, **9**, 671–675.
32 Y. M. Moustafa and K. El-Egili, *J. Non-Cryst. Solids*, 1998, **240**, 144–153.
33 P. Y. Shih, J. Y. Ding and S. Y. Lee, *Mater. Chem. Phys.*, 2003, **80**, 391–396.
34 S. Tanaka, K. Fujita, Y. Miyake, M. Miyamoto, Y. Hasegawa, T. Makino, S. Van der Perre, J. Cousin Saint Remi, T. Van Assche, G. V. Baron and J. F. M. Denayer, *J. Phys. Chem. C*, 2015, **119**, 28430–28439.
35 C. Hao, D. Zhou, J. Xu, S. Hong, W. Wei, T. Zhao, H. Huang and W. Fang, *J. Mater. Sci.*, 2021, **56**, 9434–9444.
36 M. A. Luzuriaga, C. E. Benjamin, M. W. Gaertner, H. Lee, F. C. Herbert, S. Mallick and J. J. Gassensmith, *Supramol. Chem.*, 2019, **31**, 485–490.
37 M. D. J. Velásquez-Hernández, R. Ricco, F. Carraro, F. T. Limpoco, M. Linares-Moreau, E. Leitner, H. Wiltsche, J. Rattenberger, H. Schröttner, P. Frühwirt, E. M. Stadler, G. Gescheidt, H. Amenitsch, C. J. Doonan and P. Falcaro, *CrystEngComm*, 2019, **21**, 4538–4544.
38 M. Mozafari, S. Banijamali, F. Baino, S. Kargozar and R. G. Hill, *Acta Biomater.*, 2019, **91**, 35–47.
39 H. Zhang, M. Zhao, Y. Yang and Y. S. Lin, *Microporous Mesoporous Mater.*, 2019, **288**, 109568.
40 Y. Xue, Z. Zhu, X. Zhang, J. Chen, X. Yang, X. Gao, S. Zhang, F. Luo, J. Wang, W. Zhao, C. Huang, X. Pei and Q. Wan, *Adv. Healthcare Mater.*, 2021, **10**, 2001369.
41 D. Bůžek, S. Adamec, K. Lang and J. Demel, *Inorg. Chem. Front.*, 2021, **8**, 720–734.
42 S. A. Butonova, E. V. Ikonnikova, A. Sharsheeva, I. Y. Chernyshov, O. A. Kuchur, I. S. Mukhin, E. Hey-Hawkins, A. V. Vinogradov and M. I. Morozov, *RSC Adv.*, 2021, **11**, 39169–39176.
43 V. C. Ramos, C. B. G. Reyes, G. M. García, M. I. S. Quesada, F. J. M.-C. Barrero, J. J. S. Rábago and M. S. Polo, *Pharmaceutics*, 2022, **14**, 2546.
44 I. B. Vasconcelos, T. G. D. Silva, G. C. G. Militão, T. A. Soares, N. M. Rodrigues, M. O. Rodrigues,

N. B. D. Costa, R. O. Freire and S. A. Junior, *RSC Adv.*, 2012, **2**, 9437.
45 A. Tiwari, A. Singh, N. Garg and J. K. Randhawa, *Sci. Rep.*, 2017, **7**, 12598.
46 L. Shi, J. Wu, X. Qiao, Y. Ha, Y. Li, C. Peng and R. Wu, *ACS Biomater. Sci. Eng.*, 2020, **6**, 4595–4603.
47 A. Sharsheeva, V. A. Iglin, P. V. Nesterov, O. A. Kuchur, E. Garifullina, E. Hey-Hawkins, S. A. Ulasevich, E. V. Skorb, A. V. Vinogradov and M. I. Morozov, *J. Mater. Chem. B*, 2019, **7**, 6810–6821.
48 M. Kalati and K. Akhbari, *New J. Chem.*, 2021, **45**, 22924–22931.
49 B. Milborne, A. Arjuna, M. T. Islam, A. Arafat, R. Layfield, A. Thompson and I. Ahmed, *ACS Omega*, 2024, **9**, 50933–50944.
50 H. Zhang, D. Liu, Y. Yao, B. Zhang and Y. S. Lin, *J. Membr. Sci.*, 2015, **485**, 103–111.